ANALYSIS OF TRANSIENT VIBRATIONS OF A TRUCK UNDERCARRIAGE DUE TO ROAD UNEVENNESSES

I. KUTI and P. MICHELBERGER

Department of Transport Engineering Mechanics,
Technical University of Budapest, H-1521
Received: January 10, 1988

Abstract

In the bar-model dynamic analysis of truck undercarriage frames of open-section bars, dynamic equilibrium equations in terms of either centroid or shear centre coordinates of the bar cross section are equally useful.

Results obtained in the computer analysis of transient vibrations of a truck undercarriage by the two different equilibrium equations have been compared. Also simulation of wheel bouncing while crossing a road defect has been concerned with.

Introduction

In the mechanical modelling of undercarriage frames of utility vehicles made of open-section bars, application of equilibrium equations in terms of shear centre displacements (angular rotations) of bar cross sections with the inherent shear-centre finite element network (shear centre description) has been generalized [1, 2]. Dynamic equilibrium equations of open-section bars can also be written in terms of centroidal displacements of cross sections [3] with the inherent centroidal finite element network (centroidal description).

From Fig. 2, the shear centre finite element network obviously is a less exact model for the real bar length in the undercarriage frame than the centroidal finite element network, probabilizing important deviations between internal stresses of the undercarriage frame obtained by centroidal or by shear centre description.

Transformation between shear centre and centroidal descriptions is no problem for mass and stiffness matrices obtained (by the finite element method) for open-section bars and for the generalized force vector. Derivation of the mentioned mass and stiffness matrices and of the generalized force vector by means of shear centre coordinates, that has been treated in [2, 4], will not be considered here. Only the shear centre to centroid transformation applicable for these characteristics will be outlined.

The origin of the coordinate system is put to the centroid, thereby centroidal coordinates of the represented cross section are $Y_s = 0$, $Z_s = 0$, while shear centre coordinates are Y_T and Z_T (Fig. 1). Let mass matrix, stiffness matrix and generalized force vector for the shear centre coordinates be denoted $\mathbf{M}_T$, $\mathbf{S}_T$, and $\mathbf{F}(t)_T$, respectively, while $\mathbf{M}_s$, $\mathbf{S}_s$ and $F_s(t)$ are for centroidal co-ordinates. Then transformation relationships become:

$$\mathbf{M}_s = \mathbf{A}^T \mathbf{M}_T \mathbf{A} \tag{1}$$

$$\mathbf{S}_s = \mathbf{A}^T \mathbf{S}_T \mathbf{A} \tag{2}$$

$$\mathbf{F}_s(\mathrm{t}) = \mathbf{A}^T \mathbf{F}_T(\mathrm{t}) \tag{3}$$

where: t — time dependence of generalized force vectors;
$\mathbf{A}^T$ — transposed of $\mathbf{A}$,

$$\mathbf{A} = \begin{bmatrix}
1 & & & & & & & & & & & & & \\
 & 1 & & -z_T & & & & & & & & & & \\
 & & 1 & -y_T & & & & & & & & & & \\
 & & & 1 & & & & & & & & & & \\
 & & & & 1 & & y_T & & & & & & & \\
 & & & & & 1 & -z_T & & & & & & & \\
 & & & & & & 1 & & & & & & & \\
 & & & & & & & 1 & & & & & & \\
 & & & & & & & & 1 & & -z_T & & & \\
 & & & & & & & & & 1 & y_T & & & \\
 & & & & & & & & & & 1 & & & \\
 & & & & & & & & & & & 1 & & -y_T \\
 & & & & & & & & & & & & 1 & -z_T \\
 & & & & & & & & & & & & & 1
\end{bmatrix}$$

where empty elements are zero.

Matrices $\mathbf{M}_s$, $\mathbf{M}_T$, $\mathbf{S}_s$, $\mathbf{S}_T$, $\mathbf{A}$ have 14 by 14 elements, while $\mathbf{F}_s(\mathrm{t})$, $\mathbf{F}_T(\mathrm{t})$ are vectors with 14 elements. Specific distorsion typical of warping, and the couple of moments (bimoment) due to inhibited warping are namely included explicitly as self-contained variables, elements of the generalized displacement

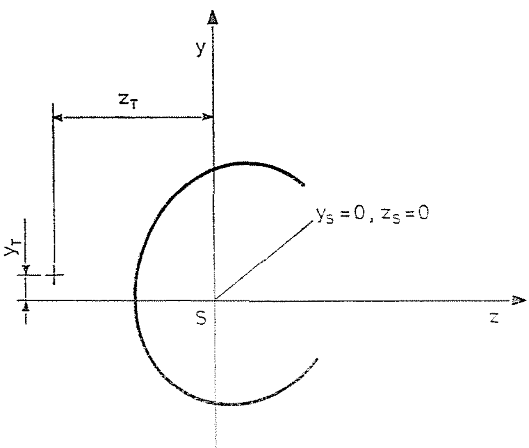

Fig. 1

vector, and force vector, respectively. Handling the specific distorsion typical of warping else than a self-contained variable, the mentioned matrices will have 12 by 12, and the generalized force vectors 12 elements [4, 5].

As concerns warping alone, at joints of open-section bar elements modelled as linear continua, either free warping or fully inhibited warping can be specified. In the real structure, nodal warpings of open-section bars are generally intermediary between the two extremes. Therefore a decision has to be made by analyzing nodal joints between the two (idealized) specifications for nedal warpings.

Analysis of transient vibrations cannot dispense with taking the effect of built-in springs and dampers, as well as of the tyre elasticity into consideration. Since only an overal picture is needed of the truck behaviour while crossing a road defect, dampers have been modelled by a linear characteristic. Since rubber tyres are much stiffer than mainsprings, linear spring characteristics suffice to model tyre elasticity. Also simulation of the material damping of rubber tyres involves dampers with linear characteristics. Hence, the undercarriage model in this study is a linear one [6, 7].

If trucks are driven on poor roads, wheels are seen to bounce off the road surface even at moderate speeds, hinting to the absolute necessity to include the possibility of wheel bouncing in the solution algorithm, lest tensile forces might arise in rubber tyres and mainsprings, significantly distorting computation results. Thereby behaviour of the mechanical model, in occurrence of wheel bounce, becomes non-linear throughout the test period, that can, however, be divided in to intervals where behaviour of the undercarriage model is linear [7].

Analysis of transient vibrations applies a variety of Wilson's method [8] permitting automatic treatment of wheel bounce. The involved finite element program has been developed at the Department of Transport Engineering Mechanics.

1. Main features of the finite element model of the tested truck undercarriage

Frame (Fig. 2) of the tested truck undercarriage (Fig. 3) is a replica of the Erz undercarriage [9] of open-section U bars. Position of the coordinate system is seen in Fig. 3.

Front and rear running gear bridges are modelled by bars of great stiffness compared to the undercarriage frame, joined at end points by springs and dampers simulating rubber tyre elasticity and material damping. Connection of built-in mainsprings and dampers to the gear and the frame is seen in Fig. 3. They are hinged to both the nodes of the shear-centre finite element network

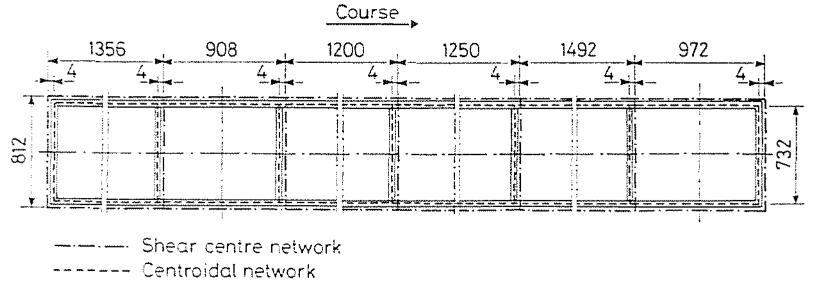

Fig. 2

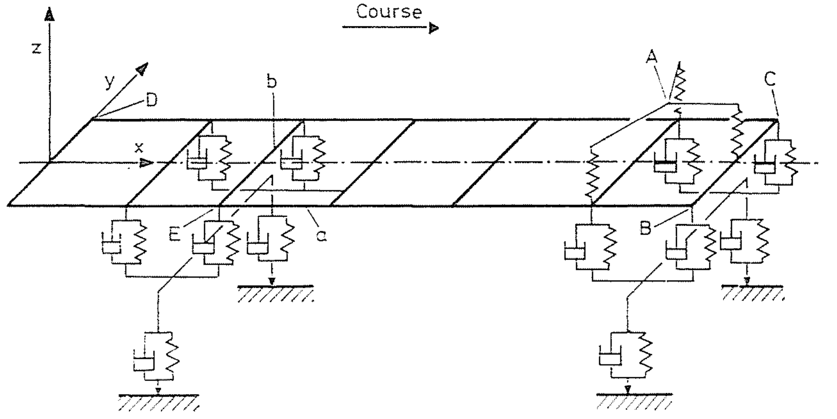

Fig. 3

and to the running gear. There by equal loads affect two springs and dampers each at one side of the running gear bridges. Figure 3 shows the shear-centre finite element network of the undercarriage frame, joined at the first segment in the advancement direction, across three springs and three highly stiff arms, by a node representing the motor and the speed box.

Warping at the undercarriage frame nodes is assumed to be mutually hindered by beams and spreaders.

The working load is 8000 kg assumed to be uniformly distributed between nodes at the four rear sections of beams. The driver's cab (with driver) weighs 1000 kg, is assumed to be uniformly distributed between nodes at the two front sections of beams. Mass of the undercarriage frame is distributed in proportion to bar section lengths between nodes of the undercarriage frame. (The finite element network has also nodes at mid-spreaders.) Motor and gearbox weigh 1250 kg, in addition, also secondary moments of inertia about axes parallel to X and Y axes crossing their common centroid (as principal axes of inertia) have been reckoned with. Front and rear gears weigh 700, and

1400 kg, resp., distributed between end points and mid-points of cross-wise horizontal bars representing front and rear bridges, so as to keep secondary moments of inertia along axes in direction X crossing mid-points equal before and after distribution. Thereby the mass matrix becomes a diagonal matrix generalized in finite element programs, while the stiffness matrix is a stripe matrix typical of the finite element method.

2. Computation data

For the analysis of transient vibrations of the tested truck undercarriage, road defect is described as:

$$U_z = 0.05(1-\cos\varphi),\ [m],\ 0 \leq \varphi \leq 2\pi \tag{4}$$

where U_z is displacement along the vertical Z-axis.

As to the transversal extension, road defects may either be

a) as narrow as to affect only wheels at one side (asymmetric road defect); or

b) as wide as to simultaneously affect the pair of right- and left-side wheels (symmetric road defect).

From Fig. 2 it appears that the relative size difference between the centroidal and the shear centre finite element networks of the tested undercarriage frame is only 1.1% length-wise, while transversally it is 11%. Therefore the two different computation methods are likely to yield greater differences between internal stresses in spreaders due to asymmetric road defects.

This assumption has been fully confirmed by computer outputs.

In case of symmetric loads due to symmetric road defects, where the principal stress results from the bending of beams about the Y-axis (Fig. 3) the relative maximum deviation between internal stress counterparts obtained by the two computation methods was less than 3% even for crossing speeds $v = 20$ km/h and $v = 60$ km/h. Crossing the symmetric road defect is exemplified in Fig. 4, showing time functions of bending moments at point E of beam a about the y-axis with the centroid as origin, for crossing speeds $v = 20$ km/h and $v = 60$ km/h.

The two computation methods yield relative difference maxima of 23 to 27% between counterpart internal stresses in spreaders symmetrically loaded by asymmetric road defects.

Time functions about the centroid for torques in spreader **b** (Fig. 3) passing over an asymmetric road defect at speeds $v = 20$ km/h, and $v = 60$ km/h are seen in Fig. 5.

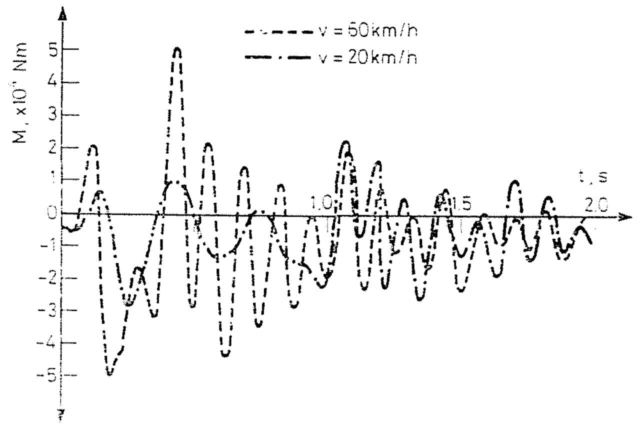

Fig. 4

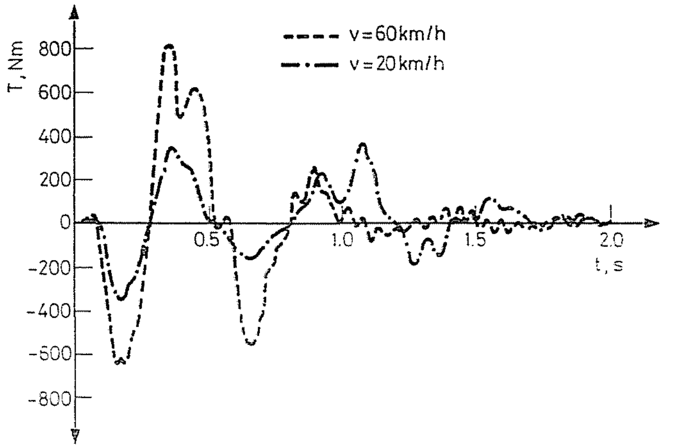

Fig. 5

Time functions of torques in spreader **b** again passing over an asymmetric road defect, plotted about the shear centre and the centroid, are shown in Fig. 6, for a passage speed $v = 20$ km/h.

The trend of variation of the bimoment function for inhibited warping in spreader **b** is the same as for the corresponding torque at either speed. (For a passage speed $v = 60$ km/h, in centroidal representation $B_{\max} = 277.5$ Nm², and for shear centre representation $B_{\max} = 224.7$ Nm² ($t = 0.35$ s)).

Counterpart nodal displacements of the two finite element models in the two different representations differ by less than 3%, so it is sufficient to present nodal displacements of one of the finite element models described in terms of e.g. centroidal coordinates.

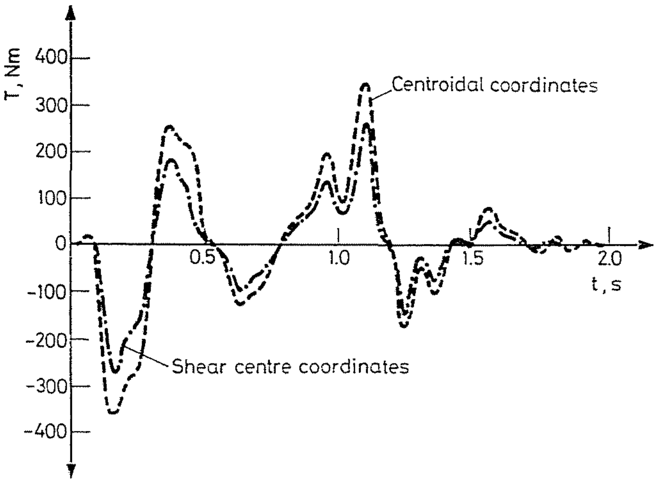

Fig. 6

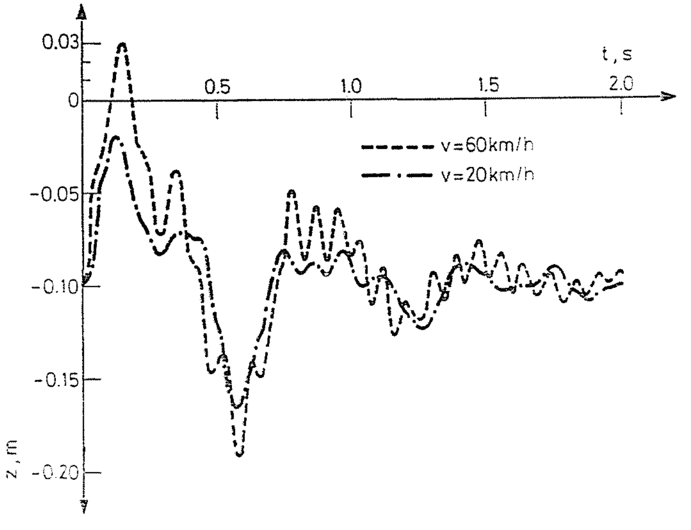

Fig. 7

Displacements vs. time of node C of the undercarriage frame due to a symmetric road defect is seen in Fig. 8 for speeds $v = 20$ km/h and $v = 60$ km/h.

Displacements vs. time of node B of the undercarriage frame due to an asymmetric road defect is seen in Fig. 8 for passage speeds $v = 20$ km/h and $v = 60$ km/h.

The critical position of wheel bounce proved to be at a speed $v = 20$ km/h both for a symmetric and for an asymmetric road defect. Time functions of the

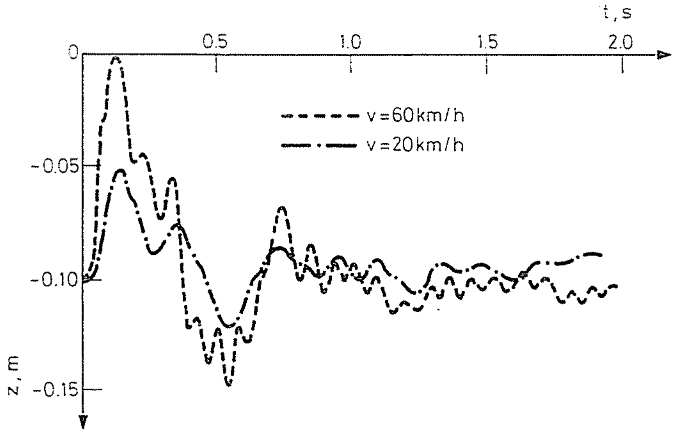

Fig. 8

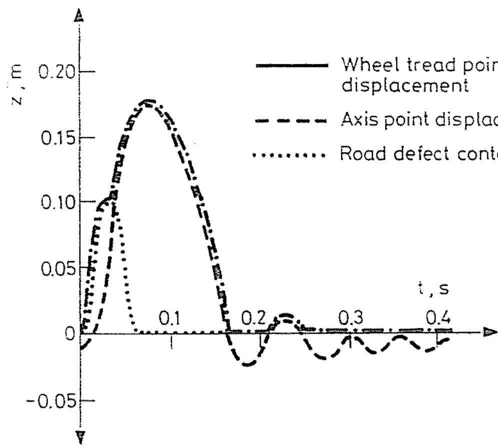

Fig. 9

front right wheel tread point and axis point displacements for a symmetric road defect are seen in Fig. 9 for a speed $v = 60$ km/h. According to the diagram, the wheel bounces twice.

It is of importance that, together with the bouncing wheel, also the part of the undercarriage frame over the wheel rises by 20 to 25% higher than in passing the road defect at a speed $v = 20$ km/h, accordingly, after the first landing of the wheel, also the undercarriage frame will vibrate at an increased amplitude (Figs 8, 9). Also stresses in the undercarriage frame due to increased vibrations significantly increase compared to those for a speed $v = 20$ km/h (Figs 4, 5). It is worth mentioning that in passing the asymmetric road defect at $v = 20$ km/h, also the other side (farther from the road defect) exhibits a slight (about 3 mm) wheel bounce.

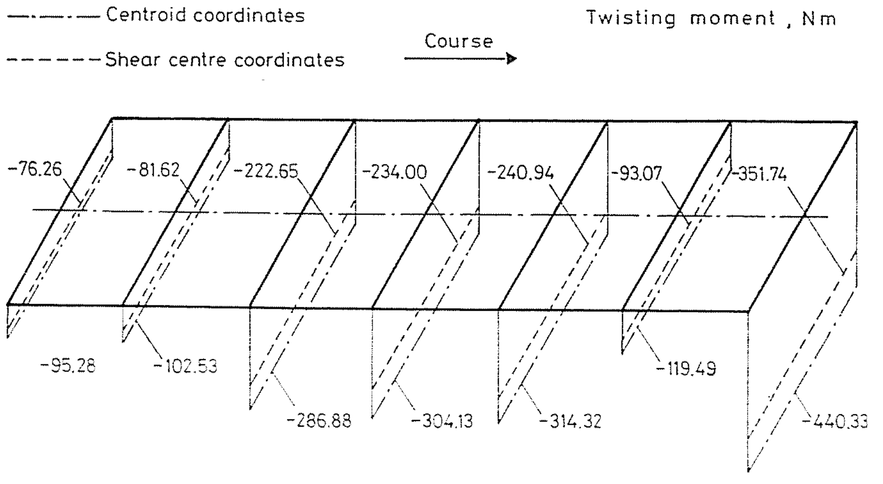

Fig. 10

The case of a nearly static load is that of the undercarriage crossing a road defect at a speed $v = 1$ km/h. Torques in spreaders crossing an asymmetric road defect at $v = 1$ km/h involving a vertical rise of 0.1 m of the right rear wheel tread point, and no vertical displacement for the other wheel tread points are seen in Fig. 10.

Conclusions drawn from computation results for finite element models involving shear centre and centroidal coordinates and geometrical network are:

a) Relative deviations of counterpart internal stresses due to symmetric loads arising from symmetric road defect are below 3%.

b) Relative deviation maxima of counterpart stresses due to asymmetric loads arising from asymmetric road defects depend on the selected bar element and the kind of stress. The maximum deviation between bending and torsional stresses in beams does not exceed 7%. Deviation between torsional stresses in spreaders may be as high as 27%. The maximum deviation computed between bending stresses (about the x-axis) in spreaders may be as high as 10%. The higher bending stress has been obtained from the shear centre finite element model.

Consequently, there is a significant, non-negligible deviation between counterpart (torsional and bending) internal stresses in spreaders due to asymmetric road defects, computable in either way. The theoretically closer value results from modelling by centroidal coordinates and finite element network compared to that by shear centre coordinates and finite element network. This statement is confirmed by the increased accuracy of the geometrical description of the modelled (real) structure by the finite element network compared to that by the shear-centre finite element network.

References

1. BEERMANN, H. J.: Static Analysis of Commercial Vehicle Frames. A Hybrid Finite Element and Analytical Method Int. Journ. of Vehicle Design, Vol. 5. No. 112. pp: 26—52 (1984).
2. VITT, D.: Berücksichtigung der Wölbtorsion bei der dynamischen Stabtragwerksberechnung. Proc. 5. Tagung Festkörpermechanik, Dresden 1982, Band B, VEB Fachbuchverlag Leipzig, pp XXV/1—XXV/10.
3. KUTI, I.: Application of the Principle of Total Potential Energy to Establish the Motion Equation of Thin-Walled Open-Section Bars, Periodica Polytechnica (Transp. Eng.), Vol. *14*, (1986), No. 1, pp. 3—16.
4. PÁCZELT, J.—HERPAI, B.: Finite Element Analysis of Bar Systems,* Műszaki Könyvkiadó, Budapest, 1987.
5. KURUTZNÉ KOVÁCS, M.: Computer Analysis of Thin-Walled, Open Cross-Section Bar Systems,* Műszaki Tudomány 53, 217—226 (1977).
6. MICHELBERGER, P.—FERENCZI, M.—ÁGOSTON, A.—UJHELYI, Z.: Dynamische Berechnung von Wagenkasten, Periodica Polytechnica (Transp. Eng.), Vol. *4*, (1976), No. 1, pp. 161—191.
7. MICHELBERGER, P.—HORVÁTH, S.: Mechanics V. In Hungarian (Selected Chapters). Tankönyvkiadó Budapest 1985.
8. BATHE, K. J.—WILSON, E. L.: Stability and Accurary Analysis of Direct Integration Methods, Int. J. of Earthquake Eng. and Struct. Dynamics, Vol. *1*, No. 2., 1973.
9. ERZ, K.: Über die durch Unebenheiten der Fahrbahn hervorgerufene Verdrehung von Strassenfahrzeugen. ATZ. *59*. 1957/4 s.98, 1957/6. s.163, 1957/11. s.345, 1957/12 s.371.

Dr. István KUTI
Dr. Pál MICHELBERGER } H-1521 Budapest

* In Hungarian.